Tripodal Peptide Hydroxamates as Siderophore Models. Iron(III) Binding with Ligands Containing H-(Alanyl)$_n$-β-(*N*-hydroxy)alanyl Strands (n = 1−3) Anchored by Nitrilotriacetic Acid

Yukihiro Hara, Langtao Shen, Akira Tsubouchi, and Masayasu Akiyama*

Department of Applied Chemistry, Tokyo University of Agriculture and Technology, Koganei, Tokyo 184-8588, Japan

Kimiko Umemoto

Department of Chemistry, International Christian University, Mitaka, Tokyo 181-8585, Japan

Received February 7, 2000

Combining three units of one of H-(alanyl)$_n$-β-(HO)alanyl peptides (n = 1−3) with nitrilotriacetic acid affords tripodal peptide hydroxamate ligands (**1L**, **1D**, **2LL**, **2DL**, and **3LLL**, where each L or D denotes the L- or D-alanyl residue). These ligands form six-coordinate octahedral complexes (Fe-**1L**, Fe-**1D**, Fe-**2LL**, Fe-**2DL**, and Fe-**3LLL**) with iron(III) in aqueous near neutral pH solution, and the stability and the chirality of the complexes formed depend on the alanyl residues incorporated. Thus Fe-**2LL** is the most stable against attack of H^+ and OH^- ions and the least labile in the iron(III) removal by EDTA. The CD spectra show a predominance of the Λ configuration for Fe-**1D**, Fe-**2LL**, Fe-**2DL**, and Fe-**3LLL**, but the opposite Δ configuration for Fe-**1L**. These ligands and their gallium(III) complexes are studied by ^{1}H NMR spectroscopy in DMSO-d_6 solution. CD and NMR spectral analysis, aided by molecular model examinations, indicates that critical factors in controlling the configuration and the stability of the complexes are (1) the hydroxamate-carrying alanyl residue, (2) the expanse of an interior space in the ligand, and (3) an interstrand amide NH hydrogen bond; the latter bonding is possible with ligands **2LL** and **2DL**. A microbial growth promotion activity test shows that ligands **1L**, **2LL**, and **3LLL** all act as iron-transporting agents.

Introduction

In microbial iron assimilation, siderophores play a prominent role for sequestering iron from the environment. Siderophores are low molecular weight iron-chelating compounds produced by microorganisms, which take up iron(III) from siderophore−iron complexes after recognition by membrane receptors.[1−7] The characteristic properties of the siderophore complexes and unique recognition behavior of microbial receptors have stimulated the design and synthesis of biomimetic siderophore analogues for better understanding of the iron coordination and microbial iron transport.[4−8] Knowledge thus accumulated will be utilized to develop clinical drugs for certain metal detoxification and furthermore to fabricate functionalized materials in artificial systems.[9,10]

A naturally abundant type of siderophore carries three bidentate hydroxamate groups in linear, cyclic, or tripodal arrangements.[4] The three hydroxamate groups coordinate to the metal ion octahedrally and create a characteristic three-dimensional shape under the influence of the supporting ligand, and the backbone of the ligand is forced into a locally restricted conformation.[4,11] Such interplay between the coordination to iron and the conformational preference of the ligand can be

(1) (a) Neilands, J. B. *Annu. Rev. Biochem.* **1981**, *50*, 715−731. (b) Neilands, J. B. *Annu. Rev. Nutr.* **1981**, *1*, 27−46. (c) Neilands, J. B. *J. Biol. Chem.* **1995**, *45*, 26723−26726.
(2) Emery, T. In *Metal Ions in Biological Systems*; Sigel, H., Ed; Marcel Dekker: New York, 1978; Vol. 7, pp 77−126.
(3) Keller-Schierlein, W.; Prelog, V.; Zähner, H. *Fortschr. Chem. Org. Naturst.* **1964**, *22*, 279−333.
(4) (a) Matzanke, B. F.; Müller-Matzanke, G.; Raymond, K. N. In *Iron Carriers and Iron Proteins*; Loehr, T. M., Ed.; Physical Bioinorganic Chemistry Series, Vol. 5; VCH Publishers: New York, 1989; pp 3−121. (b) Raymond, K. N.; Müller, G.; Matzanke, B. F. *Top. Curr. Chem.* **1984**, *123*, 49−102. (c) Matzanke, B. F. In *Encyclopedia of Inorganic Chemistry*; King, R. B., Ed.; John Wiley & Sons: Chichester, 1994; Vol. 4, pp 1915−1932.
(5) Winkelmann, G., van der Helm, D., Neilands, J. B., Eds. *Iron Transport in Microbes, Plants and Animals*; VCH Publishers: Weinheim, 1987.
(6) Winkelmann, G., Ed. *Handbook of Microbial Iron Chelates*; CRC Press: Boca Raton, FL, 1991.
(7) (a) Braun, V.; Winkelmann, G. *Prog. Clin. Biochem. Med.* **1987**, *5*, 67−99. (b) Leong, S. A.; Winkelmann, G. In *Metal Ions in Biological Systems*; Sigel, A., Sigel, H., Eds.; Marcel Dekker: New York, 1998; Vol. 35, pp 147−189.
(8) (a) Crumbliss, A. L. In *Handbook of Microbial Iron Chelates*; Winkelmann, G., Ed.; CRC Press: Boca Raton, FL, 1991; pp 177−233. (b) Albrecht-Gary, A.-M.; Crumbliss, A. L. In *Metal Ions in Biological Systems*; Sigel, A., Sigel, H., Eds.; Marcel Dekker: New York, 1998; Vol. 35, pp 239−328. (c) Shanzer, A.; Libman, J. In *Handbook of Microbial Iron Chelates*; Winkelmann G., Ed.; CRC Press: Boca Raton, FL, 1991; pp 309−338.
(9) (a) Guerinot, M. L. *Annu. Rev. Microbiol.* **1994**, *48*, 743−772. (b) Hider, R. C. *Struct. Bonding* **1984**, *58*, 25−87. (c) Bergeron, R. J., Brittenham, G. M., Eds. *The Development of Iron Chelators for Clinical Use*; CRC Press: Boca Raton, FL, 1994.
(10) Weizman, H.; Ardon, O.; Mester, B.; Libman, J.; Dwir, O.; Hadar, Y.; Chen, Y.; Shanzer, A. *J. Am. Chem. Soc.* **1996**, *118*, 12368−12375.
(11) van der Helm, D.; Jalal, M. A. F.; Hossain, M. B. In *Iron Transport in Microbes, Plants and Animals*; Winkelmann, G., van der Helm, D., Neilands, J. B., Eds.; VCH Publisher: Weinheim, 1987; pp 135−165.

10.1021/ic0001210 CCC: $19.00
Published on Web 10/06/2000

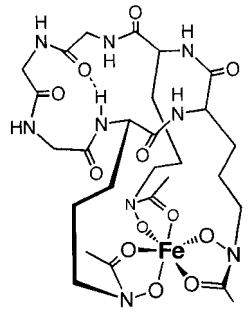

Figure 1. Ferrichrome in the Λ configuration.

explored in depth using chiral ligands which contain, for example, strands composed of α-amino acids and peptides.

Ferrichrome is a representative tripodal iron(III) complex utilized among fungi.[1,2] Its three exocyclic hydroxamate groups of the N^{δ}-acetyl-N^{δ}-hydroxy-L-ornithine residues form the iron(III) complex exclusively in the Λ-cis configuration (Figure 1).[4a,12,13] The Λ configuration is similarly taken by sequence-modified linear and cyclic ferrichrome analogues,[14] and the Δ-cis configuration has been observed for its enantiomer, the D-ornithine-derived counterpart.[15] In these instances, the ornithyl α-carbon obviously controls the disposition of the hydroxamate group. The configurational chirality of siderophore complexes has been shown as one of the important factors for cellular uptake; the retrohydroxamate ferrichrome of the Λ-configuration is biologically active,[16] as ferrichrome, but enantioferrichrome is not active for desferrichrome-producing microorganisms.[17]

In this connection, a number of biomimetic desferrichrome analogues have been synthesized, using a variety of tripodal molecules such as 1,3,5-trisubstituted benzenes,[18a−d] nitrilotriacetic acid (NTA),[18b] 2,4,6-trisubstituted cyanuric acids,[18b] tricarboxylic acids,[18b,e] trimelamol derivatives,[18f] tris(aminoethyl)amine (TREN),[18g,h] tris(hydroxymethyl)ethane and -methane,[18i,j] and 1,5,9-cyclotriazadodecane[18k] and a similar analogue.[18l] These synthetic siderophores showed a range of microbial activities when examined by growth promotion tests.[18−20] However, the thermodynamic stability, kinetic lability, and chiral tendency of these iron(III) complexes have never

Chart 1

$N[CH_2CO\text{-L-Ala-}\beta\text{-(HO)Ala-OMe}]_3$ **(1L)**

$N[CH_2CO\text{-D-Ala-}\beta\text{-(HO)Ala-OMe}]_3$ **(1D)**

$N[CH_2CO\text{-L-Ala}^1\text{-L-Ala}^2\text{-}\beta\text{-(HO)Ala-OMe}]_3$ **(2LL)**

$N[CH_2CO\text{-D-Ala}^1\text{-L-Ala}^2\text{-}\beta\text{-(HO)Ala-OMe}]_3$ **(2DL)**

$N[CH_2CO\text{-L-Ala}^1\text{-L-Ala}^2\text{-L-Ala}^3\text{-}\beta\text{-(HO)Ala-OMe}]_3$ **(3LLL)**

Scheme 1

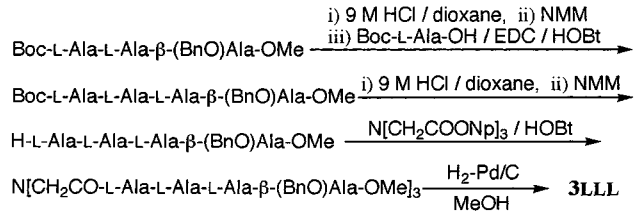

elaborately been investigated in terms of changes in ligand structures.[21] As an extension to the previous communication,[22] we have synthesized tripodal alanyl-peptide hydroxamates, **1L**, **1D**, **2LL**, **2DL**, and **3LLL**, where each **L** or **D** denotes the L- or D-alanyl residue (Chart 1), using NTA as the anchor molecule. The results of iron(III) complex formation and characteristic properties of the complexes formed are presented here, with emphasis on the effects of the alanyl residues.

Results

Design and Synthesis. We chose the alanyl (Ala) residue as the component for the present ligands, because it is a simple chiral α-amino acid, and it has an interesting helix-forming tendency.[23,24] The tris(*p*-nitrophenyl ester) of NTA[18b] was obtained in good yield via *p*-nitrophenyl trifluoroacetate. The merits in using NTA as the tripodal anchor molecule are that (1) the N-terminus of a peptide strand synthesized from the C-terminus is subjected to acylation in due course with the above activated NTA, to give the desired ligands, and (2) the NTA moiety serves formally as a glycine residue, although its nitrogen atom is shared by the three strands. The hydroxamate group was generated by use of H-*β*-(HO)Ala-OMe,[25] the 2-(methoxycarbonyl)ethyl group being the common substituent on the hydroxamate nitrogen. The benzyl (Bn), *tert*-butoxycarbonyl (Boc), and the methyl groups were used as the protective groups. The peptide units of Boc-L-Ala-*β*-(BnO)Ala-OMe and Boc-(L-Ala)$_2$-*β*-(BnO)Ala-OMe were previously obtained,[26] but Boc-D-Ala-*β*-(BnO)Ala-OMe, Boc-D-Ala-L-Ala-*β*-(BnO)Ala-OMe, and Boc-(L-Ala)$_3$-*β*-(BnO)Ala-OMe were newly prepared. Boc-(L-Ala)$_4$-*β*-(BnO)Ala-OMe was also prepared but not used because of its sparing solubility. The synthetic procedure for **3LLL** is shown in Scheme 1 as a representative example. Final deprotection of the benzyl groups by catalytic hydrogenation with a Pd−C catalyst afforded ligands **1**−**3**. They were

(12) Zalkin, A.; Forrester, J. D.; Templeton, D. H. *J. Am. Chem. Soc.* **1966**, *88*, 1810−1814.
(13) van der Helm, D.; Baker, J. R.; Eng-Wilmont, D. L.; Hossain, M. B.; Loghry, R. A. *J. Am. Chem. Soc.* **1980**, *102*, 4224−4231.
(14) Akiyama, M.; Katoh, A.; Mutoh, T. *J. Org. Chem.* **1988**, *53*, 6089−6094.
(15) Naegeli, H.-U.; Keller-Schierlein, W. *Helv. Chim. Acta* **1978**, *61*, 2088−2095.
(16) (a) Olsen, R. K.; Ramasamy, K. *J. Org. Chem.* **1985**, *50*, 2264−2271. (b) Emery, T.; Emery, L.; Olsen, R. K. *Biochem. Biophys. Res. Commun.* **1984**, *119*, 1191−1197.
(17) Winkelmann, G.; Braun, V. *FEMS Microbiol. Lett.* **1981**, *11*, 237−241.
(18) (a) Yoshida, I.; Murase, I.; Matekaitis, R. J.; Martell, A. E. *Can. J. Chem.* **1983**, *61*, 2740−2744. (b) Lee, B. H.; Miller, M. J.; Prody, C. A.; Neilands, J. B. *J. Med. Chem.* **1985**, *28*, 317−323 and 323−327. (c) Mitchell, M. S.; Walker, D.-L.; Whelan, J.; Bosnich, B. *Inorg. Chem.* **1987**, *26*, 396−400. (d) Akiyama, M.; Katoh, A.; Ogawa, T. *J. Chem. Soc., Perkin Trans. 2* **1989**, 1213−1218. (e) Karunaratne, K.; Orvig, H. C. *Tetrahedron Lett.* **1992**, *33*, 1827−1830. (f) Ramurthy, S.; Miller, M. J. *J. Org. Chem.* **1996**, *61*, 4120−4124. (g) Ng, C. Y.; Rodgers, S. J.; Raymond, K. N. *Inorg. Chem.* **1989**, *28*, 2062−2066. (h) Katoh, A.; Akiyama, M. *J. Chem. Soc., Perkin Trans. 1* **1991**, 1839−1842. (i) Tor, Y.; Libman, J.; Shanzer, A. *J. Am. Chem. Soc.* **1987**, *109*, 6518−6519. (j) Motekaitis, R. J.; Sun, Y.; Martell, A. E. *Inorg. Chem.* **1991**, *30*, 1554−1556. (k) Esteves, M. A.; Vaz, M. C. T.; Gonçalves, M. L. S. S.; Farkas, E.; Santos, M. A. *J. Chem. Soc., Dalton Trans.* **1995**, 2565−2573. (l) Gasper, M.; Grazina, R.; Bodor, A.; Farkas, E.; Santos, M. A. *J. Chem. Soc., Dalton Trans.* **1999**, 799−806.
(19) Shanzer, A.; Libman, J.; Lazar, R.; Tor, Y.; Emery, T. *Biochem. Biophys. Res. Commun.* **1988**, *157*, 389−394.
(20) Gaspar, M.; Santos, M. A.; Krauter, K.; Winkelmann, G. *BioMetals* **1999**, *12*, 209−218.
(21) Dayan, I.; Libman, J.; Agi, Y.; Shanzer, A. *Inorg. Chem.* **1993**, *32*, 1467−1475.
(22) Akiyama, M.; Hara, Y.; Gunji, H. *Chem. Lett.* **1995**, 225−226.
(23) Chou, P. Y.; Fasman, G. D. *Annu. Rev. Biochem.* **1978**, *47*, 251−276.
(24) Spek, E. J.; Olson, C. A.; Shi, Z.; Kallenbach, N. R. *J. Am. Chem. Soc.* **1999**, *121*, 5571−5572.
(25) Shimizu, K.; Akiyama, M. *J. Chem. Soc., Chem. Commun.* **1985**, 183−184.
(26) Hara, Y.; Akiyama, M. *Inorg. Chem.* **1996**, *35*, 5173−5180.

Table 1. UV−Vis Spectra, Monoprotonation Constants, and CD Spectral Data for Tris(hydroxamato)iron(III) Complexes[a]

complex	λ_{max}/nm (ϵ/M^{-1} cm^{-1})	$K_{Fe(HL)}$	CD band /nm ($\Delta\epsilon$)		type
Fe-**1L**	425 (2900)	5.1×10^6	360 (+2.5)	450 (−5.4)	Δ
Fe-**1D**	425 (2900)	nd[b]	360 (−2.6)	450 (+5.5)	Λ
Fe-**2LL**	425 (3000)	3.8×10^2	380 (−6.9)	465 (+2.2)	Λ
Fe-**2DL**	425 (3000)	2.0×10^3	377 (−7.5)	460 (+2.9)	Λ
Fe-**3LLL**	425 (3000)	8.1×10^3	380 (−3.3)	460 (+1.1)	Λ
ferrichrome[c]	430 (2900)	3.1×10^d	360 (−3.7)	465 (+2.4)	Λ

[a] Determined in water at 25.0 ± 0.1 °C at pH 7.0. The $K_{Fe(HL)}$ value was obtained according to eq 2 (text). [b] Not determined. [c] Reference 4a. [d] Reference 31.

characterized by elemental analysis, IR, and ^{1}H NMR spectroscopy, and their purity was checked by HPLC.

^{1}H NMR spectral data were obtained in DMSO-d_6 solutions. Proton signals were assigned by the aid of COSY−NOESY experiments (and the results are listed in Table S1, Supporting Information). The key observations for these ligands are as follows: (1) The α-proton of the Ala-N(OH) residue characteristically appeared downfield as a quintet at ca. δ 4.80 ppm by the influence of the electron-withdrawing N−OH group.[26] The expected intensity of this α-proton confirmed that the hydroxamic acid groups were fully present in all the ligands. (2) The temperature-dependence coefficients of amide-proton chemical shifts, determined in the range 20−30 °C, were larger in negative values (−0.004 to −0.007 ppm deg^{-1}) than that expected for intramolecularly hydrogen bonded protons (expected to be less than −0.003 ppm deg^{-1}).[27,28] The methylene groups in the NTA moiety appeared mostly as a singlet.

Iron(III) Complex Formation. Iron(III) complexes were prepared by adopting a procedure previously described.[26] An acidic mixture of a ligand in aqueous solution and an aqueous ferric nitrate solution was made (pH 2.1), which contained mostly a di(aquo)bis(hydroxamato)iron(III) species (1:2 complex of iron(III) with a hydroxamato group), $Fe(HL)^+$, having a λ_{max} of 465 nm.[29,30] The 1:2 complex was transformed into a tris(hydroxamato)iron(III) complex (1:3 complex), Fe(L), by neutralization with alkali to pH 7. The UV−vis spectra of the 1:3 complexes (Fe-**1L**, Fe-**1D**, Fe-**2LL**, Fe-**2DL**, and Fe-**3LLL**) showed their characteristic absorptions at λ_{max} 425 nm with ϵ ca. 3000 M^{-1} cm^{-1}, typical of the tris(hydroxamato)iron(III) complexes [4] (Table 1).

Iron(III) Complex Stability. Plots of their ϵ values at 425 nm vs pH show middle plateau regions where the iron(III) species is in the tris(hydroxamato) coordination (Figure 2). The spanning of the plateau gives an estimate for the stability of the tris(hydroxamato)iron(III) complexes against attack of H^+ or OH^- ions. The stability decreases in the order Fe-**2LL** (pH 4.5−10.2) > Fe-**2DL** (pH 4.5−9.5) > Fe-**3LLL** (pH 5.6−9.5) > Fe-**1L** and Fe-**1D** (pH 6.2−9.0). Ferrichrome was shown to have a wider plateau of pH 3.7−10.5.[14]

When a neutral complex solution was gradually acidified, the λ_{max} shifted to a longer wavelength and its ϵ value decreased.[27] An isosbestic point was observed, for example, for

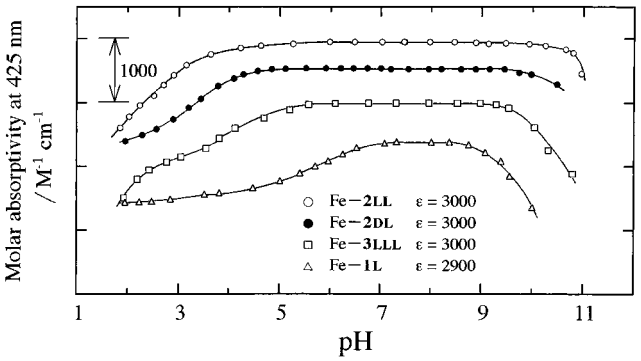

Figure 2. Absorption vs pH plots: values of ϵ/M^{-1} cm^{-1} at 425 nm in water at 25.0 °C. The scale in the ordinate is defined, but each plot is shown in an arbitrary position.

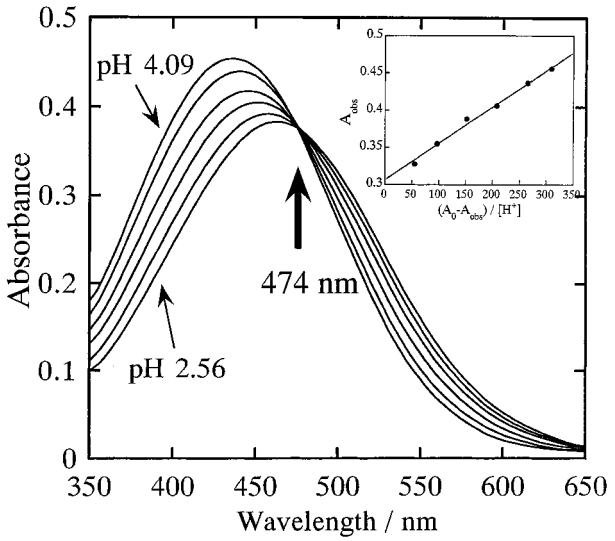

Figure 3. UV−visible spectra of Fe-**2DL** (2.62×10^{-4} M) in water at 25.0 °C, covering the pH range 2.56−4.09. The inset is a Schwarzenbach plot for the same pH range.

Fe-**2DL** at 474 nm in the given pH range, however, the third $Fe(H_2L)^{2+}$ species gradually appears with spectral deviation from the isosbestic point in going to a further lower pH region (Figure 3). Isosbestic behavior clearly indicated the equilibrium between Fe(L) and $Fe(HL)^+$ (eq 1), confirming the presence of Fe(L).

$$Fe(L) + H^+ \rightleftharpoons Fe(HL)^+ \quad (1a)$$

$$K_{Fe(HL)} = [Fe(HL)^+]/[Fe(L)][H^+] \quad (1b)$$

The equilibrium was further analyzed by applying the Schwarzenbach equation (eq 2)[29] to the isosbestic spectral data to give the monoprotonation constant ($K_{Fe(HL)}$). The resulting plot is included as the inset in Figure 3.

$$A_{obs} = (A_0 - A_{obs})/[H^+]K_{Fe(HL)} + \epsilon_{Fe(HL)}c_{total} \quad (2)$$

The values of $K_{Fe(HL)}$, whose logarithmic values represent half protonation pH values ($pH_{1/2}$), indicate the relative ease of monoprotonation of the tris(hydroxamato)iron(III) complexes (Table 1). The corresponding value reported for ferrichrome is much smaller.[31]

(27) (a) Llinás, M.; Klein, P. M.; Neilands, J. B. *J. Mol. Biol.* **1970**, *52*, 399−414. (b) Llinás, M.; Klein, P. M.; Neilands, J. B. *J. Mol. Biol.* **1972**, *68*, 265−284. (c) Llinás, M.; Klein, P. M.; Neilands, J. B. *J. Biol. Chem.* **1973**, *248*, 924−931.
(28) Ohnishi, M.; Urry, D. W. *Biochem. Biophys. Res. Commn.* **1967**, *36*, 194−202.
(29) Schwarzenbach, G.; Schwarzenbach, K. *Helv. Chim. Acta* **1963**, *46*, 1390−1400.
(30) Caudle, M. T.; Stevens, R. D.; Crumbliss, A. L. *Inorg. Chem.* **1994**, *33*, 6111−6115.
(31) Anderegg, G.; L'Eplattenier, F.; Schwarzenbach, G. *Helv. Chim. Acta* **1963**, *46*, 1409−1422.

Table 2. Iron(III) Removal Rates by EDTA and Equilibrium Data for Iron(III) Competition Reactions with EDTA[a]

complex	removal rate k_{obs}/s^{-1}	competition equilibrium unchanged/%
Fe-**1L**	1.7×10^{-1}	5.7
Fe-**1D**	1.7×10^{-1}	5.7
Fe-**2LL**	2.5×10^{-3}	14
Fe-**2DL**	1.4×10^{-2}	5.8
Fe-**3LLL**	3.0×10^{-3}	7.9
ferrichrome[b]	6.1×10^{-4}	

[a] Iron(III) removal rates were determined at 25.0 ± 0.1 °C and pH 5.4 in an acetic acid−NaOH buffer with ionic strength 0.1 (KCl): The initial concentration of tris(hydroxamato)iron(III) complexes = 1.0×10^{-4} M with a 20-fold excess of EDTA. The competition reaction for iron(III) between a ligand and EDTA was carried out with [iron(III) complex] = [EDTA] = 2.6×10^{-4} M at 25.0 ± 0.1 °C and pH 5.4. [b] Reference 14: Under similar conditions, but the initial concentration ratio was [Fe(L)]/[EDTA] = 3.8×10^{-4} M/7.6×10^{-3} M.

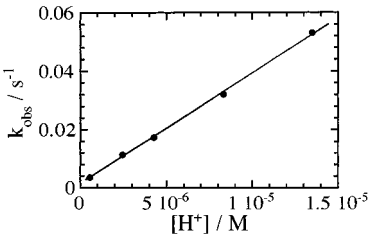

Figure 4. Rates (k_{obs}) of iron removal from Fe-**2DL** (1.0×10^{-4} M) by EDTA (20 molar excess) at 25.0 ± 0.1 °C in different pH solutions (pH 5−6).

Iron(III) Exchange Kinetics with EDTA. The iron-withholding power of these tris(hydroxamato)iron(III) complexes was assessed by iron-exchange kinetics using EDTA as a competing ligand.[32] The iron removal reaction from Fe(L) by EDTA would proceed as expressed by eq 3.[32,33] Iron(III) exists virtually as Fe(L) or $Fe(EDTA)^-$.

$$Fe(L) + H^+ \overset{K_{Fe(HL)}}{\rightleftharpoons} Fe(HL)^+ \quad (3a)$$

$$Fe(HL)^+ + H_2EDTA^{2-} \overset{K}{\rightleftharpoons} (HL)Fe(H_2EDTA)^- \xrightarrow{k_2} H_3L + Fe(EDTA)^- \quad (3b)$$

The rate (k_{obs}) of the iron-exchange reaction with excess EDTA was determined at pH 5.4 by monitoring a decrease in the absorbance of Fe(L) at 425 nm (Table 2). The removal rates decreased in the order Fe-**1L** = Fe-**1D** > Fe-**2DL** > Fe-**3LLL** > Fe-**2LL**. Under conditions of pH 7.4, we still observed a faster rate for Fe-**1L** (2.8×10^{-4} s^{-1}) than that for Fe-**2LL** (4.4×10^{-5} s^{-1}).

We further investigated the reaction to obtain information about mechanism. Figure 4 shows that the rate linearly increases with the increasing proton concentration in the pH range 5−6, for example, when Fe-**2DL** was used as Fe(L) in eq 3.

In repeat-scanning spectra for one of the reaction runs, we observed an isosbestic point at a wavelength of 350 nm (in the insert of Figure 5). The spectral change clearly indicates that two major species of Fe(L) and $Fe(EDTA)^-$ are in the solution with a low concentration of the intermediate species $(HL)Fe(H_2EDTA)^-$. Examination of the effect of changing EDTA concentrations on the iron removal from Fe-**2LL** revealed a hyperbolic curvature (Figure 5).[26,33] This saturation behavior is expressed by eq 3c, using eqs 3a and 3b.

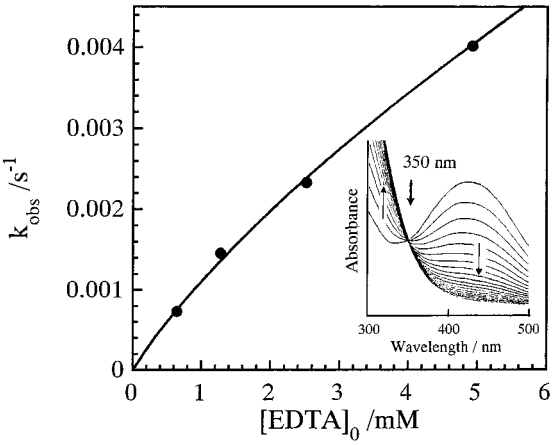

Figure 5. Dependence of the iron(III) removal rates of Fe-**2LL** on EDTA concentrations at pH 5.4 and 25.0 ± 0.1 °C: Fe-**2LL**, 1.3×10^{-4} M. The inset shows spectral changes for one of the runs conducted with 2.6 mM EDTA.

$$\text{rate} = k_{obs}[Fe(L)] = k_2[(HL)Fe(H_2EDTA)^-] \quad (3c)$$

where

$$k_{obs} = k_2[(HL)Fe(H_2EDTA)^-]/[Fe(L)] = k_2K'[H_2EDTA^{2-}]/(1 + K'[H_2EDTA^{2-}])$$

and

$$K' = KK_{Fe(HL)}[H^+]/(1 + K_{Fe(HL)}[H^+])$$

We obtained values of $K = 99$ M^{-1} and $k_2 = 1.2 \times 10^{-2}$ s^{-1}.

Exchange Equilibrium with EDTA. The proton-independent stability constant ($K_{Fe(L)}$) of Fe(L) is defined by eq 4. This constant is obtainable from the proton-dependent equilibrium constant (K_{eq}) of a ferric ion competition reaction between a ligand (H_3L) and EDTA,[4,31] when the ligand protonation constants are known. The equilibrium reaction with the constant K_{eq} is expressed by eqs 5a and 5b.

$$Fe^{3+} + L^{3-} \rightleftharpoons Fe(L), \quad K_{Fe(L)} = Fe(L)/[Fe^{3+}][L^{3-}] \quad (4)$$

$$Fe(L) + H_2EDTA^{2-} + H^+ \rightleftharpoons H_3L + Fe(EDTA)^- \quad (5a)$$

$$K_{eq} = [H_3L][Fe(EDTA)^-]/[Fe(L)][H_2EDTA^{2-}][H^+] \quad (5b)$$

Equimolar competition reactions expressed by eq 5a were performed at pH 5.4 and 25 °C, and the amounts of the unexchanged iron complexes were determined spectrophotometrically on the basis of the stoichiometry of reaction 5a; the unexchanged iron complexes increased in the order Fe-**1L** = Fe-**1D** < Fe-**2DL** < Fe-**3LLL** < Fe-**2LL** (Table 2).

We were unable to determine the ligand protonation constants owing to hydrolysis of the ester group during the titration, hence the proton-independent stability constants for the present complexes were not obtained.

Chirality of Complexes. The circular dichroism (CD) spectra of the complexes in aqueous neutral solution exhibited Cotton effects (Table 1), as shown typically for an enantiomeric pair of Fe-**1L** and Fe-**1D** (Figure 6). From the spectral patterns, the Δ and Λ configurations around the metal ion were assigned to

(32) Tufano, T. P.; Raymond, K. N. *J. Am. Chem. Soc.* **1981**, *103*, 6617−6624.
(33) Albrecht-Gary, A.-M.; Palanche-Passeron, T.; Rochel, N.; Hennard, C.; Abdallah, M. A. *New J. Chem.* **1995**, *19*, 105−113.

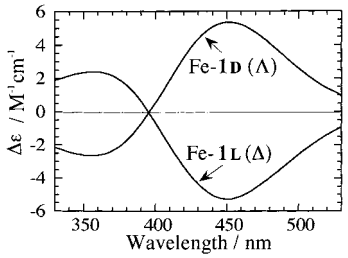

Figure 6. CD spectra of Fe-**1L** and Fe-**1D** in water at pH 7.0: $\Delta\epsilon$ (M^{-1} cm^{-1}) vs λ/nm.

Fe-**1L** and Fe-**1D**, respectively, by reference to the assignment for ferrichrome.[12,13] Some notable observations are as follows: (1) in the confines of the L-alanyl peptide series the configuration changes; Fe-**1L** has the Δ configuration, whereas Fe-**2LL** and Fe-**3LLL** have the Λ configuration; (2) the magnitudes of CD intensities (from the peak top to the trough) are different depending on the number of alanyl residues; (3) the CD intensity of Fe-**2DL** is larger than that of Fe-**2LL**; and (4) these intensities are larger than that of ferrichrome [4a] except for Fe-**3LLL**.

NMR Spectra of Ga(III) Complexes. In general, Ga(III) complexes are structurally similar to the corresponding Fe(III) complexes but are diamagnetic.[27,34,35] The present Ga(III) complexes were prepared according to the reported procedure.[27] Their ^{1}H NMR spectra were obtained in DMSO-d_6 solutions, and signals were assigned by the aid of COSY−NOESY experiments. (Results are summarized in Table S1.) Relative to the ligands, some of proton signals from the corresponding Ga(III) complexes were shifted; in all the Ga complexes examined, NCH_2CO− protons appeared as AB q patterns, and shifted downfield except for those of Ga-**3LLL**. All the N*H* Ala^1 protons shifted downfield, while N*H* Ala^2 of Ga-**2DL** shifted upfield, N*H* Ala^2 of Ga-**3LLL** was unchanged, but N*H* Ala^2 of Ga-**2LL** slightly shifted downfield. N*H* Ala^3 of Ga-**3LLL** was upfield shifted. The four protons from the C-terminal −N(O$^-$)-CH_2CH_2CO− moiety shifted downfield in all the complexes. The temperature dependence of amide proton chemical shifts were determined between 20 and 30 °C. (The results are also included in Table S1.) Compared to the free ligands, some of the NH proton shifts showed less dependence on temperature, indicating the presence of intramolecularly hydrogen bonded structures. Smaller temperature coefficients (−0.0012 to −0.0023 ppm deg^{-1}) were observed for N*H* Ala^1 of both Ga-**2LL** and Ga-**2DL**, and N*H* Ala^2 and N*H* Ala^3 of Ga-**3LLL**. Conformational change upon complex formation is also indicated in some of the $^3J_{NH-\alpha H}$ values (Table S1).

The NOE data for the complexes were measured at mixing times of 400, 600, and 800 ms, and observed major NOEs are depicted in Figure 7. Particularly noteworthy are the strong inter-residue NOE's observed for NH^1−NH^2 in Ga-**2LL** and NH^2−NH^3 in Ga-**3LLL**. Difference in the structures of Ga-**2LL** and Ga-**3LLL** is manifested in the NOE from CH^1, which is close to NH^2 in Ga-**2LL**, whereas it is not to NH^2 in Ga-**3LLL**.

IR Spectra of Fe(III) Complexes. The IR bands for the amide absorption for all the iron(III) complexes appeared at 1650 and 1580 cm^{-1} (KBr disk).

Growth Promotion Activity. The activity was examined by a reported procedure using an *Escherichia coli* K-12 RW 193 mutant (ATCC 33475)[36] as a test organism.[37] This mutant cannot synthesize enterobactin, but grows when supplied with iron(III) by suitable artificial siderophores, because it has several receptors including the FhuA protein for ferrichrome uptake.[38] The growth promotion activity of Fe-**1L**, Fe-**2LL**, and Fe-**3LLL** was equally weak (+), in comparison with strong activity (+++) of ferrichrome.

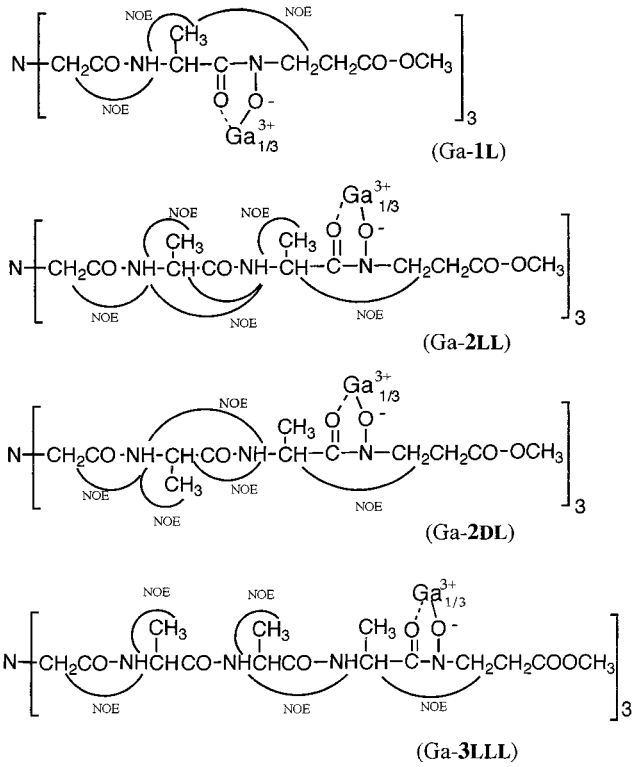

Figure 7. ^{1}H NMR NOE data for Ga(III) complexes of ligands **1L**, **2LL**, **2DL**, and **3LLL**.

Discussion

Ligands. Despite their peptide nature, the ligands are not structured in a polar solvent like DMSO. In NMR spectra, the NCH_2CO− protons appeared as singlets except for a doublet for **1L**, consistent with freely extended conformations, and temperature-dependence coefficients of large negative values for the amide protons indicated the absence of intramolecular hydrogen bonds. The ligands, therefore, are not preorganized for iron complexation[39] in water of high polarity, in which intramolecular hydrogen bond formation is strongly inhibited.

Fe(III) Complexes. (a) General. The five iron(III) complexes containing oligoalanyl residues were examined in terms of the four experimental categories: (1) the monoprotonation stability, (2) the stability against attack of H^+ or OH^- ions, (3) the exchange equilibrium thermodynamics, and (4) the lability in iron(III) removal kinetics. The following increasing stability order was observed for categories 1−3: Fe-**1L** = Fe-**1D** < Fe-**2DL** ≤ Fe-**3LLL** < Fe-**2LL**. The decreasing kinetic lability order was observed for category 4: Fe-**2LL** > Fe-**3LLL** > Fe-**2DL** > Fe-**1L** = Fe-**1D**.

These iron(III) complexes are more kinetically labile and thermodynamically less stable than ferrichrome.[14] Ferrichrome holds iron through its flexible side chains, whereas the present

(34) Borgias, B. A.; Barclay, S. J.; Raymond, K. N. *J. Coord. Chem.* **1986**, *15*, 109−123.
(35) Dietrich, A.; Fidelis, K. A.; Powell, D. R.; van der Helm, D.; Eng-Wilmot, D. L. *J. Chem. Soc., Dalton Trans.* **1991**, 231−239.
(36) Wayne, R.; Frick, R.; Neilands, J. B. *J. Bacteriol*. **1976**, *126*, 7−12.
(37) Neilands, J. B. *Struct. Bonding* **1984**, *58*, 1−24.
(38) Braun, V.; Hantke, K.; Köster, W. In *Metal Ions in Biological Systems*; Sigel, A., Sigel, H., Eds.; Marcel Dekker: New York, 1998; Vol. 35, pp 67−145.
(39) Cram, D. J. *Science* **1988**, *240*, 760−767.

ligands bind iron(III) with peptide hydroxamate groups. Peptides have their own conformational tendencies, which are not necessarily suitable for flexible iron(III) binding, with the consequence that iron complexes become less stable and kinetically more labile.

(b) Exchange Kinetics. At pH 5.4, Fe-**1L** and Fe-**1D** contain a considerable amount of the protonated species Fe(HL), whereas Fe-**2LL**, Fe-**3LLL**, and Fe-**2DL** exist as Fe(L) (Figure 2). The protonation to Fe-**1L** and Fe-**1D** is not the single cause for the faster rate, however, since a faster rate for Fe-**1L** than that for Fe-**2LL** was observed even at a higher pH of 7.4.

As expressed by eq 3a, the protonation of Fe(L) is a necessary first step. This is supported by the observation of a linear dependence of the rate on the proton concentration in the pH range 5−6 (Figure 4). The hyperbolic dependence of the rates (Figure 5) indicates saturation kinetics by which the iron(III) removal reaction proceeds through the formation and breakdown of the intermediate ternary complex (eq 3b) and indicates that the rate-determining step is the breakdown rather than the formation of the intermediate.[33] The curved line is a calculated one which gives the values of K and k_2. The K value in 3a involves the process of formation of the bis(hydoxamato) complex to breakdown of the monohydroxamato complex. A similar mechanism has previously been discussed for iron(III) removal from the peptide hydroxamate complexes.[26]

(c) Iron(III) Exchange Equilibrium. The proton-independent stability constants for similar tris(hydroxamato)iron(III) complexes differ only slightly in many cases. For example, the constants of ferrichrome and tris(acetohydroxamato)iron(III) are $10^{29.1}$ and $10^{28.3}$, respectively,[31] and that of Fe-**2LL** was previously estimated to be 10^{29}. For comparison of the stability of the present complexes, we assume that every ligand has a similar set of the three hydroxamate protonation constants. This is reasonable, because every tripodal ligand has each alanyl hydroxamic acid moiety located at the C-terminal position and, being unstructured, experiences protonation influences in the same manner. Thus, an increase in the amount of the unexchanged complexes is directly proportional to an increase in the K_{eq} value and hence in the stability constant. Thus, a small range of the stability differences observed by changing the alanyl residues are real in the present situation.

Structure of Complexes. (a) General Features. General structural features of the present complexes, as emerged from the IR and NMR data with the aid of molecular model work with CPK or HGS,[40] are the following. (1) The amide bonds are in the trans coplanar conformation. This is based on the IR absorption observed at 1650 cm^{-1} for the amide carbonyl groups of the iron complexes. On the other hand, the cis amide bonds, for example, present in *N*-hydroxy diketopiperazines, absorb at higher frequencies of 1680−1690 cm^{-1} in the solid state (KBr disk).[41] (2) Only one set of NMR signals were observed, demonstrating C_{3v} symmetry of the complexes. Together with this fact, it is demanded that hydroxamato group must be in the cis orientation with respect to each other, to coordinate octahedrally to the metal ion. (3) The nitrilotriacetyl moiety assumes an extended (a zigzag type) conformation with its nitrogen lone-pair electrons directed inward to accommodate the metal ion. (4) In the L-alanyl unit that constitutes the hydroxamate carbonyl group, the Λ configuration places the C^{α}−H bond nearly cis to the C(O)−N bond that is one edge of the five-membered chelate ring, whereas the Δ configuration places the C^{α}−CH_3 bond nearly cis to the C(O)−N bond; in the latter case, steric interaction between the side chain methyl and the β-methylene protons becomes pronounced. The hydroxamate-carrying alanyl residue is a critical determinant for the configuration, and in most cases the side chain methyl of the L-Ala-NO^- moiety forces the complex to assume the Λ configuration, so as to avoid contact with the β-protons of the propanoate moiety.

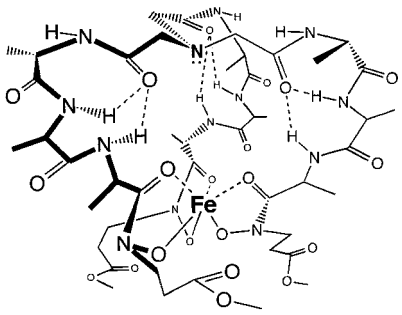

Figure 8. Possible structure for Fe-**3LLL** of the Λ configuration, showing hydrogen bonds formed and the electron pair direction on the nitrogen: this structure is built with the aid of the CD and NMR data; the alanyl residue ϕ and φ angles are listed in Table 3.

Table 3. Angles (ϕ, φ) Adopted and $^3J_{NH-\alpha H}$ Values for Metal(III) Complex Structures[a]

	ϕ, φ; J /Hz		
complex	Ala[1] (D-Ala[1])	L-Ala[2]	L-Ala[3]
M-**1L**	−80, −140; J = 7.5		
M-**2LL**	−90, −80; J = 8.9	−90, 140; J = 8.9	
M-**2DL**	90, −120; J = 8.2	−90, 160; J = 7.9	
M-**3LLL**	0, 40; J = 2.8	−90, −60; J = 8.6	−130, 140; J = 10.1

[a] Metal(III) corresponds to Fe(III) or Ga(III). The ϕ (=θ + 60), φ angles adopted in the model building obtained via the dihedral angles θ (not shown) derived from the $^3J_{NH-\alpha H}$ values using a Karplus type equation.

The $^3J_{NH-\alpha H}$ values of the Ga(III) complexes provided information about the dihedral angles θ. Using a Karplus type equation, a set of angles ϕ were derived from θ,[42] and adaptable angles ϕ were determined. The CD and these NMR data, combined with the above structural features, provide possible structures for the individual iron(III) complexes of Fe-**1**, Fe-**2** (**LL** and **DL**), and Fe-**3LLL**. Fe-**3LLL** is shown as a representative one in Figure 8. (Structures Fe-**2** (**LL** and **DL**) are depicted in Figure S1 (Supporting Information), and structure Fe-**1L** is depicted in the synopsis (Table of Contents).) Table 3 gives a list of the angles ϕ and φ adopted for building these structures.

(b) Individual Complexes. The result that Fe-**1L** and Fe-**1D** are the least stable and the most labile is reasonable, considering their shortest length of the strand which has to assume a strained compact structure. Fe-**1L** has the Δ configuration. Ga-**1L** shows an NOE between the side chain methyl and β-protons of the propanoate moiety, together with that between the NCH_2CO− and the N*H* Ala protons (Figure 7). This is consistent with the Δ configuration, where the C^{α}−CH_3 bond is oriented nearly cis to the C(O)−N(O) bond. This seemingly unfavorable configuration cannot be avoided so as to retain a sufficient space for iron accommodation; a further rotation of nearly 120° would bring the C^{α}−H bond nearly cis to the C(O)−N(O) bond, but

(40) A set of miniature molecular models, sold from Maruzen, Tokyo. These models allow concomitant rotation of several bonds linking to a bond of interest and are also usable as space-filling models.

(41) Akiyama, M.; Katoh, A.; Tsuchiya, Y. *J. Chem. Soc., Perkin Trans. 1* **1989**, 235−239.

(42) Bystrov, V. F.; Portnova, S. L.; Balashova, T. A.; Koz'min, S. A.; Gavrilov, Y. D.; Afanas'ev, V. A. *Pure Appl. Chem.* **1973**, *36*, 19−34.

the interior space would become much smaller. In the Ramachandran diagram,[43] the Ala residue is found far outside the β-sheet region, indicative of strain. Hydrogen bond networks may not be formed in such a rigid structure, as not observed for this complex.

In Ga-**2**, that is, Fe-**2** (**2LL** and **2DL**) complexes, the strand becomes more flexible by one added alanine residue, thereby the interior space becomes expanded relative to that of ligand **1** and the unfavorable Δ configuration is avoided. The observed NOE signals between the α-proton of the L-Ala-NO$^-$ moiety and the β-protons of the propanoate moiety are consistent with this configuration (Figure 7). For Ga-**2LL**, Ala^1 is found near the π-helix and Ala^2 in the β-sheet region in the Ramachandran diagram. For both **2LL** and **2DL** complexes, intramolecular hydrogen bonds are formed across the two neighboring strands between the nitrilotriacetyl carbonyl and the NH Ala^1 proton (C═O···HN), stabilizing the entire conformation of the complexes. Intramolecular hydrogen bonding certainly stabilizes ferrichrome structure.[13,14]

The stability order suggests, however, that there are some other factors which destabilize complexes Fe-**2DL** and Fe-**3LLL** relative to Fe-**2LL**. The presence of both D-residue and L-residue in Ga-**2DL**, and similarly in Fe-**2DL**, forces the strand to assume a sharp turn at the D-alanyl α-carbon atom ($\phi \approx 90°$ and $\varphi \approx -120°$), leaving an interior space narrower than that of Ga-**2LL** and consequently decreasing the stability. Both D-Ala^1 and L-Ala^2 are found in the β-sheet region for Ga-**2DL**.

Fe-**3LLL** certainly has the Λ configuration. In Ga-**3LLL** $^3J_{NH-\alpha H}$ values for Ala^1 and Ala^3 take extreme values of 2.8 and 10.1 Hz, indicating that the molecular structure is rigid and that the conformation of these residues is constrained. This is the manifestation of destabilization of Fe-**3LLL**. Specifically, the dihedral angle HN−αH (θ) in Ala^1 is practically fixed to about −60°, whereas that of Ala^3 is fixed to about 170° (±20°). On the other hand, Ala^1 or Ala^2 in Ga-**2LL** is not particularly constrained as judged from the $^3J_{NH-\alpha H}$ values. From the NOE data for Ga-**3LLL** (Figure 7), close contacts are found between the N*H* Ala^2 and Ala^3 protons, in addition to the contact between α-C*H* Ala^3 and a β-proton of the propanoate group, resulting from the Λ configuration. The dihedral angle and the interresidue contact strains bring both N*H* Ala^2 and Ala^3 protons pointing inward and within a hydrogen-bonding distance to the carbonyl oxygen of the NCH$_2$−CO− moiety (intrastrand hydrogen bonding), as indicated by a small amide NH temperature-dependence coefficient. This hydrogen bonding makes the structure inflexible, but may not contribute to an increase in the stability. A model thus constructed indicates that the L-Ala^1-L-Ala^2-L-Ala^3- sequence in Fe-**3LLL** has a helical-like conformation, where Ala^1 is not in an allowed region, Ala^2 is in the α-helical region, and Ala^3 is in the β-sheet region. Thus, strain concentrates on the Ala^1 conformation upon complexation. If a complex is formed with the nitrogen lone-pair electrons pointing out, the whole structure becomes congested and more NOE cross peaks are expected than actually observed.

The twist angles (60° for a regular octahedron and 0° for a trigonal prism)[11] of the metal ion coordination are estimated for these structures, whose magnitudes decrease in the order Fe-**2DL**, Fe-**2LL**, and Fe-**3LLL**. This order is in line with the observed order of CD intensities. Such a correlation seems to hold under the limited circumstance of the present molecular arrangement, where only numbers of alanine residues change. A twist angle of 43° has been observed for ferrichrome,[13] interestingly, whose CD intensity is intermediate between those of Fe-**2LL** and Fe-**3LLL**.

Biological Activity. The weak but positive biological activity observed for both Λ and Δ configurational isomers could be ascribed to either (1) a less selective recognition for ferrichrome derivatives by the FhuA protein or (2) a case in which a different receptor might be used, since *E. coli* has many types of receptors.[7,38] A weak discrimination was observed against enantioferrichrome.[17,38] In view of a test result that a NTA-based tripodal iron(III) complex, Fe^{III}−N[CH$_2$CONHCH$_2$CH$_2$-CH$_2$N(O$^-$)COCH$_3$]$_3$, is utilized by RW 193 but not by a mutant devoid of the FhuA receptor,[18b] we tentatively favor case 1 above.

Conclusions

Tripodal peptide ligands **1**−**3** containing different numbers of alanyl residues were synthesized using nitrilotriacetic acid as the anchor molecule to model ferrichrome. These ligands formed tris(hydroxamato) complexes with iron(III), and the complexes were investigated in terms of the conformational, configurational, and chemical properties such as protonation and iron-exchange stabilities and iron-removal kinetics. These properties changed depending on the alanyl residues incorporated. In the series, one-Ala residue ligands cannot afford a sufficiently wide metal-binding space, producing the least stable and most labile complex. The Fe-**2LL** complex was the most stable and the least labile. Fe-**2DL** also exhibited considerable stability and less kinetic lability. Two Ala residues, therefore, provided suitable metal-binding environments, but Ala residues did not assume helical conformations. In a three-Ala ligand, Ala^2 exhibited a helix-forming trait, but Ala^1 was forced to take a usually not-allowed conformation, the iron complex formed being not stabilized relative to Fe-**2LL**. In all, even Fe-**2LL** was less stable and more kinetically labile than ferrichrome. However, the purpose of this paper to observe the interplay between the iron(III) coordination, and the ligand structure was accomplished by changing the number and the chirality of alanyl residues. The iron complexes of ligands **1**−**3** containing one, two, and three L-alanyl residues, respectively, showed a similar degree of siderophore activity, although weak, for a mutant, *E. coli* K 12 RW 193.

Experimental Section

General Procedures. The melting points are uncorrected. FT-IR spectra were recorded on a JASCO model FT/IR-5M spectrophotometer. UV−vis spectra were obtained on a Hitachi 320A spectrophotometer. CD spectra were taken with a JASCO J-720 spectrophotometer. HPLC was carried out on a JASCO 880-PU apparatus combined with 875-UV and 100-III attachments, using a column (4.6 × 250 mm) of Finepac SIL C$_{18}$. A solvent system of CH$_3$CN−H$_2$O (3:1 v/v) containing 0.1% phosphoric acid was applied at a flow rate of 1 cm^3/min, and the retention time (t_R) was determined. Optical rotations were measured with a Horiba SWPA-2000 polarimeter at 25 °C. ^{1}H NMR spectroscopy was carried out in CDCl$_3$ or DMSO-d_6 with a JEOL FX-200, GX-270 and EX-400, A-500 and a Varian INOVA500 spectrometer using tetramethylsilane (TMS) as an internal standard.

Boc-D-Ala-*β*-(BnO)Ala-OMe was obtained by a procedure similar to that used for Boc-L-Ala-β-(BnO)Ala-OMe[26] using Boc-D-Ala-OH: ^{1}H NMR (CDCl$_3$) δ 1.28 (3H, d, J = 6.8 Hz, CH$_3$), 1.45 (9H, s, *t*-Bu), 2.58 (2H, t, J = 6.8 Hz, NCH$_2$C*H*$_2$CO), 3.61 (3H, s, OCH$_3$), 3.7−4.2 (2H, m, NC*H*$_2$CH$_2$CO), 4.73 (1H, m, α-CH), 4.94 (2H, m, PhC*H*$_2$), 5.28 (1H, d, J = 8.3 Hz, NH), 7.40 (5H, m, Ph).

Boc-D-Ala-L-Ala-*β*-(BnO)Ala-OMe. This was obtained, using Boc-L-Ala-β-(BnO)Ala-OMe[26] and Boc-D-Ala-OH, as an oil in 82% yield:

(43) IUPAC−IUB Commission on Biochemical Nomenclature. *Biochemistry* **1970**, *9*, 3471−3479. See also, for example: Voet, D.; Voet, J. G. *Biochemistry*; John Wiley & Sons: New York, 1990; Chapter 7.

HPLC t_R 3.6 min; IR (KBr, cm^{-1}) 1739 (C═O, ester), 1714 (C═O, urethane), 1658 (C═O, amide), 1513 (NH, amide); ^1H NMR ($CDCl_3$) δ 1.29 (3H, d, $J = 7.0$ Hz, CH_3), 1.37 (3H, d, $J = 7.3$ Hz, CH_3), 1.45 (9H, s, *t*-Bu), 2.58 (2H, t, $J = 6.6$ Hz, NCH_2CH_2CO), 3.62 (3H, s, OCH_3), 3.7−4.2 (2H, m, NCH_2CH_2CO), 4.25 (1H, m, α-CH), 4.9−5.1 (4H, m, Ph CH_2, α-CH, Boc-N*H*), 6.71 (1H, br d, NH), 7.40 (5H, m, Ph).

Boc-L-Ala-L-Ala-L-Ala-β-(BnO)Ala-OMe. Boc-Ala-Ala-β-(BnO)-Ala-OMe (3.0 g, 6.64 mmol) was treated with 8.9 M HCl/dioxane (22.4 mL) for 6 h at 0 °C and evaporated to give an amorphous solid. The solid, Boc-L-Ala-OH (1.38 g, 7.31 mmol), *N*-methylmorpholine (NMM) (0.80 mL, 7.31 mmol), 1-hydroxybenzotriazole (HOBt) (1.22 g, 7.97 mmol), and 1-ethyl-3-[3-(dimethylamino)propyl]carbodiimide hydrochloride (EDC·HCl) (1.53 g, 7.97 mmol) were dissolved in CH_2Cl_2 (50 mL) at −10 °C, and the mixture was stirred for 3 h at −10 °C, and for 24 h at room temperature, and then evaporated. The resulting solid was dissolved in EtOAc (200 mL) and washed with 5% $NaHCO_3$, 5% citric acid, and brine, then dried (Na_2SO_4), and evaporated. An amorphous solid obtained was purified by reprecipitation from hexanes−EtOAc to give the product (2.65 g, 76%): HPLC t_R 3.2 min; IR (KBr, cm^{-1}) 1740 (C═O, ester), 1707 (C═O, urethane), 1658 and 1635 (C═O, amide), 1544 (NH, amide); ^1H NMR ($CDCl_3$) δ 1.20−1.40 (9H, m, 3 × CH_3), 1.45 (9H, s, *t*-Bu), 2.58 (2H, t, $J = 6.7$ Hz, NCH_2CH_2-CO), 3.60 (3H, s, OCH_3), 3.65−4.60 (4H, m, N−CH_2CH_2 and 2 × α-CH), 4.90−5.00 (3H, m, PhCH_2, α-CH), 5.15 (1H, br d, NH), 6.82 (1H, br d, NH), 6.95 (1H, br d, NH), 7.40 (5H, m, Ph).

Tris(*p*-nitrophenyl) Nitrilotriacetate. A solution of trifluoroacetic anhydride (37.8 g, 180 mmol) and *p*-nitrophenol (20.8 g, 150 mmol) in THF (100 mL) was heated at reflux for 6 h, the solution being concentrated to dryness to give ***p*-nitrophenyl trifluoroacetate** as an oil (29.2 g, 83%): IR (KBr, cm^{-1}) 1806 (C═O, ester), 1530 (NO_2), 1347 (NO_2); ^1H NMR ($CDCl_3$) δ 7.48 (2H, 2 × *m*-H to NO_2 group), 8.48 (2H, 2 × *o*-H to NO_2 group). A solution of nitrilotriacetic acid (1.46 g, 7.7 mmol) and *p*-nitrophenyl trifluoroacetate (5.40 g, 23 mmol) in dry pyridine (10 mL) was stirred for 24 h at room temperature and then concentrated to dryness. Recrystallization of the residue from hexanes−EtOAc yielded needles of tris(*p*-nitrophenyl) nitrilotriacetate (TNPA) (2.7 g, 63%): mp 163−164 °C (lit.[18b] mp 161−162 °C); IR (KBr, cm^{-1}) 1775 (C═O, ester), 1520 (NO_2), 1347 (NO_2).

Synthetic Procedures for Protected Tripodal Ligands. The Boc group of Boc-$(Ala)_n$-β-(BnO)Ala-OMe was removed by treatment with 9 M HCl/dioxane for a few hours at 0 °C, and the solvent was removed. The residue was dissolved in DMF, and excess HCl was neutralized with NMM at 0 °C. To this were added TNPA and HOBt, the mixture being stirred for 3 days at 40 °C and the solvent removed. The residue was taken up in EtOAc, washed several times with 10% Na_2CO_3, water, and brine, and then dried (Na_2SO_4). Evaporation of the solvent gave the crude product, which was purified by column chromatography on silica gel with $CHCl_3$−MeOH (10:1 v/v).

N[CH_2CO-L-Ala-β-(BnO)Ala-OMe]$_3$ (Bn-1L). A solid of Bn-**1L** (0.27 g, 98%) was obtained starting with Boc-L-Ala-β-(BnO)Ala-OMe (0.32 g, 0.85 mmol) and TNPA (0.157 g, 0.28 mmol): HPLC t_R 4.2 min; IR (KBr, cm^{-1}) 1738 (C═O, ester), 1647 (C═O, amide), 1552 (NH, amide); ^1H NMR ($CDCl_3$) δ 1.35 (9H, d, 3 × CH_3), 2.60 (6H, m, 3 × NCH_2CH_2), 3.35 (6H, m, 3 × NCH_2CO), 3.60−4.40 (15H, m, 3 × CH_3 of ester and 3 × NCH_2CH_2), 4.80−5.20 (9H, m, 3 × α-CH of Ala and 3 × CH_2Ph), 7.40 (15H, m, 3 × Ph), 8.50 (3H, d, 3 × NH).

N[CH_2CO-D-Ala-β-(BnO)Ala-OMe]$_3$ (Bn-1D). A solid of Bn-**1D** (0.52 g, 86%) was prepared from Boc-D-Ala-β-(BnO)Ala-OMe (0.71 g, 1.87 mmol) and TNPA (0.346 g, 0.624 mmol).

N[CH_2CO-(L-Ala)$_2$-β-(BnO)Ala-OMe]$_3$ (Bn-2LL). An amorphous solid of Bn-**2LL** (2.06 g, 66%) was obtained starting with Boc-(L-Ala)$_2$-β-(BnO)Ala-OMe (3.54 g, 7.8 mmol) and TNPA (1.45 g, 2.61 mmol): HPLC t_R 2.8 min; IR (KBr, cm^{-1}) 1740 (C═O, ester), 1650 (C═O, amide), 1546 (NH, amide); ^1H NMR ($CDCl_3$) δ 1.25−1.45 (18H, m, 6 × CH_3), 2.59 (6H, m, 3 × NCH_2CH_2), 3.30−3.60 (6H, m, 3 × NCH_2-CO), 3.62 (9H, s, 3 × OCH_3), 3.63−4.27 (6H, m, 3 × NCH_2CH_2), 4.50 (3H, m, 3 × α-CH), 4.90−5.03 (9H, m, 3 × α-CH of Ala and 3 × CH_2Ph), 7.01 (3H, d, $J = 7.8$ Hz, 3 × NH), 7.40 (15H, m, 3 × Ph), 8.23 (3H, d, $J = 7.8$ Hz, 3 × NH).

N[CH_2CO-D-Ala-L-Ala-β-(BnO)Ala-OMe]$_3$ (Bn-2DL). An amorphous solid of Bn-**2DL** (0.52 g, 60%) was obtained starting with Boc-D-Ala-L-Ala-β-(BnO)Ala-OMe (0.100 g, 2.20 mmol) and TNPA (0.41 g, 0.73 mmol): HPLC t_R 3.2 min; IR (KBr, cm^{-1}) 1738 (C═O, ester), 1648 (C═O, amide), 1534 (NH, amide); ^1H NMR ($CDCl_3$) δ 1.25−1.45 (18H, m, 6 × CH_3), 2.59 (6H, m, 3 × NCH_2CH_2), 3.30−3.60 (6H, m, 3 × NCH_2CO), 3.62 (9H, s, 3 × OCH_3), 3.63−4.27 (6H, m, 3 × NCH_2CH_2), 4.50 (3H, m, 3 × α-CH), 4.90−5.03 (9H, m, 3 × α-CH and 3 × CH_2Ph), 7.01 (3H, d, $J = 7.8$ Hz, 3 × NH), 7.40 (15H, m, 3 × Ph), 8.23 (3H, d, $J = 7.8$ Hz, 3 × NH).

N[CH_2CO-(L-Ala)$_3$-β-(BnO)Ala-OMe]$_3$ (Bn-3LLL). A solid of Bn-**3LLL** (0.26 g, 58%) was obtained starting with Boc-(L-Ala)$_3$-β-(BnO)-Ala-OMe (0.496 g, 0.957 mmol) and TNPA (0.177 g, 0.32 mmol): HPLC t_R 2.7 min; IR (KBr, cm^{-1}) 1738 (C═O, ester), 1645 (C═O, amide), 1542 (NH, amide); ^1H NMR (DMSO-d_6) δ 1.10−1.30 (27H, 9 × CH_3), 2.59 (6H, m, 3 × NCH_2CH_2), 3.30 (6H, m, 3 × NCH_2CO), 3.53 (9H, s, 3 × OCH_3), 3.60−4.20 (6H, m, 3 × NCH_2CH_2), 4.32 (6H, m, 6 × α-CH), 4.79 (3H, m, 3 × α-CH), 4.80−5.00 (6H, m, 3 × CH_2Ph), 7.42 (15H, m, 3 × Ph), 7.98 (6H, d, $J = 7.3$ Hz, 6 × NH), 8.22 (3H, d, $J = 7.7$ Hz, 3 × NH).

General Procedure for Tripodal Hydroxamate Ligands by Hydrogenolysis of Benzyl Protective Groups. Each of the above obtained protected hydroxamate ligands was dissolved in MeOH and hydrogenated with H_2 in the presence of Pd−C (10%, an equal weight to a substrate) for ca. 36 h at room temperature. The catalyst was removed by filtration. Evaporation of the solvent, followed by gel-chromatography purification with an HW-40 column (MeOH) afforded the desired product as a solid.

N[CH_2CO-L-Ala-β-(HO)Ala-OMe]$_3$ (1L). An amorphous solid of **1L** (0.31 g, 95%) was obtained from Bn-**1L** (0.45 g, 0.46 mmol): HPLC t_R 2.3 min; IR (KBr, cm^{-1}) 1725 (C═O, ester), 1620 (C═O, amide), 1530 (NH, amide). Anal. Calcd for $C_{27}H_{45}O_{15}N_7 \cdot {}^3/_4H_2O$: C, 44.97; H, 6.50; N, 13.60. Found: C, 45.15; H, 6.83; N, 13.39. Optical rotation: $[\alpha]^{25}_D$ −30.4 (*c* 1.0 in MeOH).

N[CH_2CO-D-Ala-β-(HO)Ala-OMe]$_3$ (1D). An amorphous solid of **1D** (0.34 g, 91%) was obtained from Bn-**1L** (0.51 g, 0.52 mmol): HPLC t_R 2.3 min; IR (KBr, cm^{-1}) 1725 (C═O, ester), 1620 (C═O, amide), 1530 (NH, amide). Anal. Calcd for $C_{27}H_{45}O_{15}N_7 \cdot H_2O$: C, 44.69; H, 6.53; N, 13.51. Found: C, 44.49; H, 6.67; N, 13.31. Optical rotation: $[\alpha]^{25}_D$ +31.4 (*c* 1.0 in MeOH).

N[CH_2CO-(L-Ala)$_2$-β-(HO)Ala-OMe]$_3$ (2LL). An amorphous solid of **2LL** (1.26 g, 89%) was obtained from Bn-**2LL** (1.82 g, 1.52 mmol): HPLC t_R 2.2 min; IR (KBr, cm^{-1}) 1735 (C═O, ester), 1640 (C═O, amide), 1540 (NH, amide). Anal. Calcd for $C_{36}H_{60}O_{18}N_{10} \cdot H_2O$: C, 46.05; H, 6.66; N, 14.92. Found: C, 46.02; H, 6.68; N, 14.85. Optical rotation: $[\alpha]^{25}_D$ −52.7 (*c* 1.0 in MeOH).

N[CH_2CO-D-Ala-L-Ala-β-(HO)Ala-OMe]$_3$ (2DL). An amorphous solid of **2DL** (0.31 g, 79%) was obtained from Bn-**2DL** (0.51 g, 0.43 mmol): HPLC t_R 2.2 min; IR (KBr, cm^{-1}) 1735 (C═O, ester), 1650 (C═O, amide), 1535 (NH, amide). Anal. Calcd for $C_{36}H_{60}O_{18}N_{10} \cdot {}^9/_5H_2O$: C, 45.35; H, 6.72; N, 14.69. Found: C, 45.64; H, 6.79; N, 14.39. Optical rotation: $[\alpha]^{25}_D$ +13.1 (*c* 1.0 in MeOH).

N[CH_2CO-(L-Ala)$_3$-β-(HO)Ala-OMe]$_3$ (3LLL). An amorphous solid of **3LLL** (0.148 g, 92%) was obtained from Bn-**3LLL** (0.20 g, 0.143 mmol): HPLC t_R 2.2 min; IR (KBr, cm^{-1}) 1735 (C═O, ester), 1640 (C═O, amide), 1540 (NH, amide). Anal. Calcd for $C_{45}H_{75}O_{21}N_{13} \cdot 2H_2O$: C, 46.19; H, 6.81; N, 15.56. Found: C, 46.13; H, 6.91; N, 15.56. Optical rotation: $[\alpha]^{25}_D$ −72.0 (*c* 1.0 in MeOH).

Iron(III) Complex Formation. A stock solution of ferric nitrate (1.79×10^{-3} M) in 0.1 M nitric acid was prepared, and the concentration was determined by the bismuth method[44] with EDTA. Double-distilled deionized water was used to prepare the stock solution of each ligand at a concentration of approximately 8×10^{-3} M. A solution of each iron(III) complex was prepared by mixing the above ferric nitrate with the corresponding ligand solution, KNO_3 solution (1.0 M), and water. The constant temperature was maintained at 25.0 ± 0.1 °C during the determinations of CD and UV−vis spectra.

(44) Kotrlý, S.; Vřešťál, J. *Collect. Czech. Chem. Commun.* **1960**, *25*, 1148−1163. Bieber, B.; Večeřa, Z. *Collect. Czech. Chem. Commun.* **1961**, *26*, 2081−2085.

(a) An iron(III) complex solution (3.00 mL, 2.51×10^{-4} M), prepared from the ferric nitrate solution (0.42 mL, 7.52×10^{-7} mol), 1.0 M KNO_3 solution (0.30 mL), and a ligand (7.7×10^{-7} mol) in water, was measured for its CD spectrum, after the pH of the solution was adjusted with 0.1 M KOH to pH 7.4 and diluted to 3.00 mL.

(b) An iron(III) complex solution (2.50 mL, 1.50×10^{-4} M), prepared from the above 2.51×10^{-4} M solution (1.50 mL) by diluting with 0.10 M KNO_3 solution (1.00 mL), was used for measurements of its UV−vis spectrum. The pH of the solution was varied toward acid by serial addition of 0.01 or 0.1 M HNO_3 solution, or toward alkali with 0.01 or 0.1 M KOH solution, and the UV−vis spectrum was recorded at each of the different pH values.

(c) A Schwarzenbach plot was made using the data of solutions that exhibited an isosbestic point in the UV−vis spectra during serial acidification.

Rates of Iron(III) Exchange with EDTA. An iron(III) complex solution (1.50 mL of the above 2.50×10^{-4} M solution, 3.75×10^{-7} mol) was diluted with a buffer solution (1.20 mL) and 1 M KNO_3 (0.30 mL) in a 10 mm cell. This solution was kept in a cell compartment held at 25.0 °C. To initiate an exchange reaction, an aqueous solution (0.25 M) of EDTA (0.030 mL, 7.5×10^{-6} mol) was added, and a decrease in absorbance at 425 nm was monitored with time. A pseudo-first-order rate constant was obtained from a logarithmic plot of the absorbance vs time; most of the plots of this type were linear for at least more than two half-lives. The observed rate (k_{obs}) was obtained as the average value of more than two determinations with error limits of ±5%. Buffer solutions at pH 5.4 and 7.4 were prepared by dissolving the acid−base combination of acetic acid−NaOH and of tris−hydrochloric acid, respectively, in water.

Biological Assay. This was performed by a standard procedure using the paper-disk method[37] with a mutant, *E. coli* K 12 RW 193 (ATCC 33475). A bacto nutrient agar medium containing 2.0 mM ethylenediamine-di(*o*-hydroxyphenylacetic acid) was applied. The mutant was laid over the nutrient agar plates, and then filter paper disks were placed on them. Each disk was impregnated with an aliquot of an aqueous iron complex solution (10 μL of 1.00×10^{-3} M). Water was used as the blank. The diameter of the growth response zone that appeared around the disk was measured after incubation for 24 h at 37 °C. Diameters more than 30 mm were indicated as (+++) and 12−18 mm as (+) in the text.

Acknowledgment. We thank Dr. Katsuhiko Kushida, Varian Japan Co., Tokyo, for assistance in the determination of some of the NMR spectra.

Supporting Information Available: Table S1 containing ^{1}H NMR spectral data for ligands and Ga(III) complexes and Figure S1 depicting structures of Fe-**2LL** (Λ) and Fe-**2DL** (Λ). This material is available free of charge via the Internet at http://pubs.acs.org.

IC0001210